NANO LETTERS
pubs.acs.org/NanoLett Letter

Influence of Magnetic and Electric Fields on Universal Conductance Fluctuations in Thin Films of the Dirac Semimetal Cd_3As_2

Run Xiao, Saurav Islam,* Wilson Yanez, Yongxi Ou, Haiwen Liu, Xincheng Xie, Juan Chamorro, Tyrel M. McQueen, and Nitin Samarth*

Cite This: Nano Lett. 2023, 23, 5634−5640 Read Online

ACCESS | Metrics & More | Article Recommendations | Supporting Information

ABSTRACT: Time-reversal invariance (TRS) and inversion symmetry (IS) are responsible for the topological band structure in Dirac semimetals (DSMs). These symmetries can be broken by applying an external magnetic or electric field, resulting in fundamental changes to the ground state Hamiltonian and a topological phase transition. We probe these changes using universal conductance fluctuations (UCF) in the prototypical DSM, Cd_3As_2. With increasing magnetic field, the magnitude of the UCF decreases by a factor of $\sqrt{2}$, in agreement with numerical calculations of the effect of broken TRS. In contrast, the magnitude of the UCF increases monotonically when the chemical potential is gated away from the charge neutrality point. We attribute this to Fermi surface anisotropy rather than broken IS. The concurrence between experimental data and theory provides unequivocal evidence that UCF are the dominant source of fluctuations and offers a general methodology for probing broken-symmetry effects in topological quantum materials.

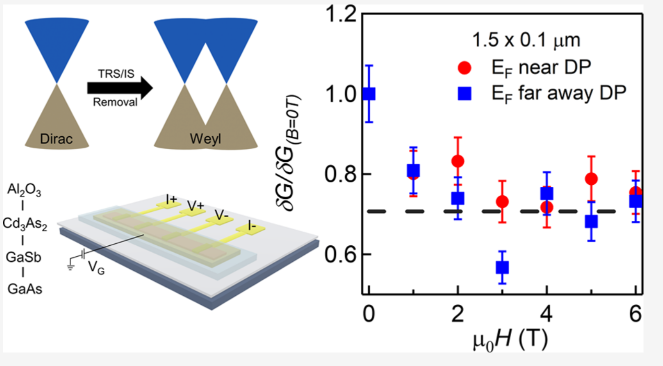

KEYWORDS: *universal conductance fluctuations, Dirac semimetal, molecular beam epitaxy, cadmium arsenide*

The past decade has seen enormous interest in the study of topological band structures created by the interplay between fundamental symmetries and strong spin−orbit coupling in a variety of quantum materials.[1−5] Dirac semimetals, a three-dimensional analogue of graphene, are an important subset in this materials class, characterized by Dirac states in the bulk with degenerate Weyl nodes that are protected by the presence of both time-reversal symmetry (TRS) and inversion symmetry (IS).[3,5] The response of Dirac semimetals to applied electrical and magnetic fields has been a matter of active discourse, in bulk crystals,[6−12] thin films,[13−20] and patterned micro-/nanostructures.[21−24] An important question in this context is whether one can experimentally observe the expected transformation of a Dirac semimetal into a Weyl semimetal in a given material when the degeneracy of the Weyl nodes is removed by breaking the TRS in an external magnetic field. Although angle-resolved photoemission spectroscopy (ARPES) could, in principle, be used to observe such a topological phase transition, it is technically impractical because of the need for a magnetic field. The observation of qualitative changes in the magnetoresistance in a Dirac semimetal at large external magnetic field has provided strongly suggestive evidence for the field-induced transition to a Weyl semimetal in $ZrTe_5$,[25] but this is still not definitive. We propose that the measurement of universal conductance fluctuations (UCF) potentially provides a more rigorous route to answering this question.[26]

UCF, a consequence of quantum interference, are aperiodic, reproducible fluctuations of the conductance of magnitude $\sim e^2/h$ in a system, observed when the sample length is comparable to the phase coherence length (L_ϕ) .[27−31] The magnitude of UCF is strongly influenced by the underlying symmetries of the system and has been used to probe the ground state symmetries in many materials.[32−40] Theory predicts that the magnetic-field-induced topological phase transition from a Dirac semimetal to a Weyl semimetal will manifest as a reduction in UCF magnitude by $\sqrt{2}$[26] as one breaks TRS. However, prior experiments have shown an approximate reduction by a factor of $2\sqrt{2}$.[23] Applying an electric field to a Dirac semimetal can also break IS. The effect of this symmetry-breaking perturbation on UCF in a Dirac semimetal is of equal fundamental importance to that of broken TRS but remains unexplored. Here, we address the

Received: March 28, 2023
Revised: June 5, 2023
Published: June 15, 2023

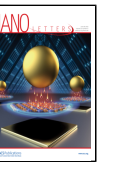

Downloaded via PENNSYLVANIA STATE UNIV on March 22, 2024 at 15:27:15 (UTC).
See https://pubs.acs.org/sharingguidelines for options on how to legitimately share published articles.
ACS Publications © 2023 American Chemical Society

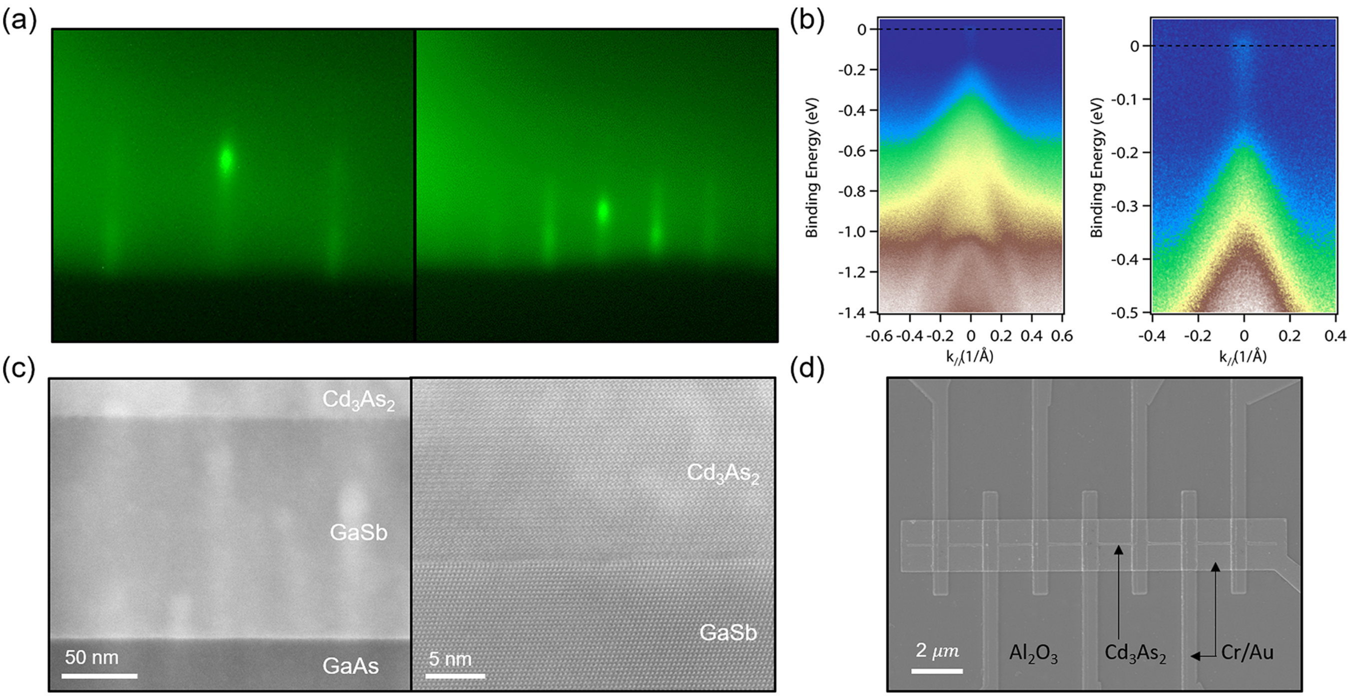

Figure 1. Material growth and device fabrication. (a) RHEED images captured during the growth of Cd_3As_2 films. The electron beam is directed along $[\bar{2}11]$(left) and $[0\bar{1}1]$ (right). (b) ARPES spectra of a 10 nm thick Cd_3As_2 film grown using similar conditions (substrate temperature, beam flux) as the thicker samples measured in transport. The measurements are taken at T = 300 K along the $\bar{K} - \bar{\Gamma} - \bar{K}$ direction. The right panel shows a slightly enlarged view of the data in the left panel. (c) Cross-sectional HAADF-STEM image of a 20 nm Cd_3As_2 film. (d) Scanning electron microscope image of a typical mesoscopic device.

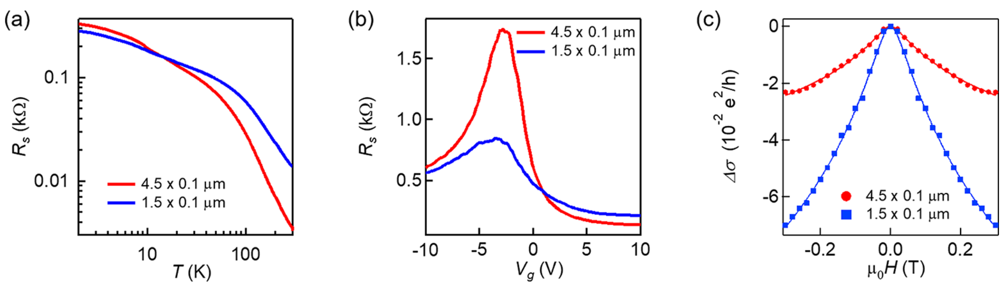

Figure 2. Basic electrical characterization. (a) Sheet resistivity (R_s) vs temperature (T) of Dev I and Dev II, both showing insulating behavior. (b) Resistance as a function of gate voltage (V_g) of Dev I and Dev II at T = 0.41 K, exhibiting charge neutrality points at V_g = −2.8 and −3.1 V, indicating that the devices are n-doped. (c) Quantum correction to conductivity ($\Delta\sigma$) as a function of the magnetic field (B) in both devices, exhibiting weak antilocalization at V_g = 0 V. The blue and red lines show a fit to the data using eq 1.

effect of applying both magnetic and electric fields to UCF in epitaxially grown thin films of the protypical Dirac semimetal Cd_3As_2, patterned into nanowires. We observe a factor of $\sqrt{2}$ reduction in UCF amplitude as the TRS is broken with application of a magnetic field, consistent with theoretical predictions. We also observe a monotonic enhancement of the UCF magnitude as the chemical potential is increased by using electrostatic gating. We argue that this most likely arises from Fermi surface anisotropy. Our experiments provide unambiguous proof of UCF to be the intrinsic source of fluctuations in mesoscopic Cd_3As_2 devices and further establish its suitability for probing topological phase transitions.

Our experiments used Cd_3As_2 films (20 nm thickness) grown by molecular beam epitaxy (MBE) on semiinsulating (111) GaAs substrates after the deposition of a 100 nm thick buffer layer of GaSb. During the growth of Cd_3As_2, we used a high-purity compound source of Cd_3As_2 in a standard effusion cell and a beam equivalent pressure of 1.2×10^{-7} Torr; the substrate temperature was 110 °C (calibrated using band-edge infrared thermometry). We have established that these growth conditions in our MBE chamber yield Cd_3As_2 films of good structural and electronic quality oriented in the [112] direction.[20] *In situ* reflection high-energy electron diffraction (RHEED) measurements showed streaky patterns in both $[\bar{2}11]$(left) and $[0\bar{1}1]$ directions, indicating reasonably ordered growth (Figure 1a). The presence of a Dirac cone in MBE-grown Cd_3As_2 films synthesized under nominally identical conditions is confirmed by *in vacuo* ARPES measurements performed after using a vacuum suitcase to transfer films from the MBE chamber to a local measurement chamber. The ARPES measurements were carried out at T = 300 K using excitation by the 21 eV helium Iα spectral line from a helium plasma lamp isolated via a monochromator and detection of emitted photoelectrons using a Scienta-Omicron DA 30L analyzer with a spectral resolution of 6 meV. As shown in Figure 1b, the ARPES data show the expected linearly

https://doi.org/10.1021/acs.nanolett.3c01174
Nano Lett. 2023, 23, 5634−5640

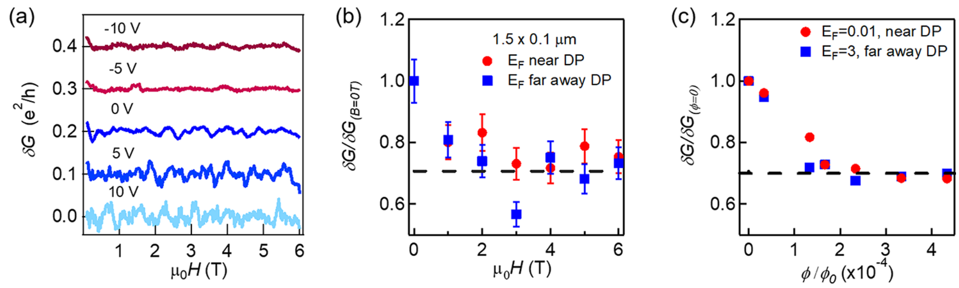

Figure 3. Magnetic-field dependence of UCF. (a) Conductance fluctuations obtained by sweeping the magnetic field at different gate voltages. (b) Magnitude of the fluctuations, normalized with the value at $B = 0$ T, showing a reduction by a factor of $\sqrt{2}$ in Dev I. The dashed line corresponds to $\sqrt{2}$ reduction. (c) Calculated UCF magnitude as a function of the normalized magnetic flux ϕ/ϕ_0 when the Fermi energy is both at the Dirac point and away from it. When the magnetic flux goes beyond a critical value, UCF magnitude decreases by $\sqrt{2}$, consistent with the experimental data.

dispersing Dirac bands, consistent with previous ARPES measurements from the (112) surface in cleaved bulk samples[41−43] and thin films.[19] We note that calculations and quantum transport measurements[20] of similar [112]-oriented Cd_3As_2 thin films indicate that a small quantum-confinement-induced gap should be expected at the Dirac point for 20 nm thick films studied here, but our ARPES measurements do not have the resolution to measure this gap. High-angle annular dark-field scanning transmission electron microscopy (HAADF-STEM) images obtained in the cross section confirm the growth of crystalline Cd_3As_2 films in the correct phase, as shown in Figure 1c.

To fabricate the mesoscopic nanowire devices investigated in this manuscript, we used electron beam lithography to first pattern and deposit 10/30 nm Cr/Au electrodes using e-beam evaporation. This was followed by another round of lithography and Argon plasma etching to pattern the nanowires. To control the chemical potential, we used a top gate with a 30 nm Al_2O_3 dielectric layer deposited by using atomic layer deposition. A scanning electron micrograph of a typical device is shown in Figure 1d. The transport measurements were performed by using a standard four-probe ac technique with a lock-in amplifier in a pumped He-3 Oxford Heliox system. We used a constant current circuit with an excitation current of 10 nA to reduce Joule heating and a carrier frequency of 17.777 Hz.

The temperature dependence of the sheet resistivity (R_s) of these films shows insulating behavior, with R_s increasing monotonically as temperature T is reduced[44] (Figure 2a). R_s as a function of gate voltage (V_g), measured in two channels of length $L = 4.5$ μm (Dev I) and 1.5 μm (Dev II) and width $W = 0.1$ μm, shows maxima at $V_g = -2.8$ and -3.1 V, respectively, referred to as the charge neutrality point (CNP), indicating the sample to be n-doped (Figure 2b). The typical mobilities of these films are $\sim 10^4$ $cm^2/(V\ s)$ at low T.[45,46] The quantum correction of conductivity for both channels show weak antilocalization, as expected for a spin−orbit coupled system (Figure 2c).[47−52] In the case of strong spin−orbit coupled systems such as Cd_3As_2, where ($\tau_\phi \gg \tau_{so}, \tau_e$), the quantum correction to conductivity ($\Delta\sigma$) can be fitted with the Hikami−Larkin−Nagaoka (HLN) equation,[48] given as

$$\triangle\sigma = \alpha\frac{e^2}{\pi h}\left[\psi\left(\frac{1}{2} + \frac{B_\phi}{B}\right) - \ln\left(\frac{B_\phi}{B}\right)\right] \tag{1}$$

Here, B_ϕ is the phase coherence field and α is a fitting parameter. The phase coherence length L_ϕ can be extracted using $L_\phi = \sqrt{\hbar/4eB_\phi}$, where e and $\hbar$ are the electronic charge and reduced Planck's constant, respectively. Both channels show comparable $l_\phi \approx 200$ nm at $V_g = 0$ V (see the Supporting Information for additional data).

Conductance fluctuations reported in this article were investigated by capturing the four-probe resistance as a function of magnetic field and gate voltage. The UCF magnitude ($\delta G = \sqrt{\langle (G - \langle G\rangle)^2\rangle}$) is defined as the rms magnitude of the variance of the fluctuations, calculated after subtracting the background by fitting a polynomial. The fluctuations are aperiodic and reproducible, which are key features of UCF (see section SII in the Supporting Information for additional data).

To probe the effect of breaking TRS, we recorded R by sweeping the magnetic field at different gate voltages, as shown in Figure 3a. We chose two V_g windows: (a) when V_g is close to the CNP (−5 to 0 V) and (b) when V_g is away from the CNP (6 to 10 V). As a function of perpendicular magnetic field, we found that the magnitude of UCF is reduced by a factor of $\sqrt{2}$, in both gate-voltage windows, as shown in Figure 3b.

Within the framework of random matrix theory (RMT),[32,33,35] the magnitude of UCF within a phase-coherent box is proportional to

$$\langle\delta G_\phi^2\rangle \propto \left(\frac{e^2}{h}\right)^2\frac{ks^2}{\beta} \tag{2}$$

Here β, s, and k are the Wigner−Dyson parameter (dependent on the universality class of the system), the degeneracy of the system under investigation, and the number of independent eigenmodes of the Hamiltonian, respectively. The value of β is 1, 2, or 4 for the orthogonal, unitary, and symplectic symmetry classes, respectively. The application of a magnetic field removes TRS, splitting the degenerate Dirac points into a pair of Weyl points (in momentum space). This leads to a transition from the Gaussian symplectic class to the unitary symmetry class. In this scenario, s changes from 2 to 1 due to the removal of Kramers degeneracy, while β changes from 4 to 2. This results in a factor of $\sqrt{2}$ reduction in UCF magnitude as the magnetic field is increased. Microscopically, the self-intersecting Cooperon modes are suppressed as the magnetic field is applied, leading to a reduction of the number of transport modes by a factor of $\sqrt{2}$. In this scenario, the fluctuations arise due to the classical diffuson modes. From a

https://doi.org/10.1021/acs.nanolett.3c01174
Nano Lett. 2023, 23, 5634−5640

heuristic analysis, the UCF magnitude starts to decrease when the magnetic field exceeds $B_0 = A(h/e)L_\phi^2$, where A depends on thermal length L_T and spin−orbit coupling length L_{so}. Normally, the factor of $\sqrt{2}$ reduction in UCF magnitude occurs only when $B \gg B_0$, and the critical field B_c for this factor of 2 reduction can be obtained from the conductance autocorrelation function. The value of B_c largely depends on the temperature and commonly increases rapidly with temperature.[53−56]

For further validation, we also performed numerical calculations of the UCF magnitude based on a $\boldsymbol{k}\cdot\boldsymbol{p}$ model developed in ref 26. We adopt the following minimal 4 × 4 Hamiltonian H_0 to describe the 3D Dirac semimetal Cd_3As_2

$$H_0(\mathbf{k}) = \begin{pmatrix} M(\mathbf{k}) & A\mathbf{k}_+ & D\mathbf{k}_- & 0 \\ A\mathbf{k}_- & -M(\mathbf{k}) & 0 & 0 \\ D\mathbf{k}_+ & 0 & M(\mathbf{k}) & -A\mathbf{k}_- \\ 0 & 0 & -A\mathbf{k}_+ & -M(\mathbf{k}) \end{pmatrix} \tag{3}$$

with $M(\mathbf{k}) = M_0 - M_z k_z^2 - M_x k_x^2 - M_y k_y^2$ and $k_\pm = k_x \pm i k_y$. A and D are the strength of spin−orbital coupling between the inverted bands $\pm M(\mathbf{k})$ and the two $M(\mathbf{k})$ orbitals, respectively. A real-space version of $H_0(\mathbf{r})$ on a discretized lattice, $H_0(\mathbf{k})$, is obtained through a Fourier transformation. The externally applied magnetic field $\vec{B}$ enters H_0 through a Piers substitution, e.g., for a magnetic field applied along the z direction, $t_x \to t_x e^{i\phi}$, where ϕ measures the magnetic flux through a unit lattice square. The disordered Cd_3As_2 material is modeled using $H = H_0 + U(\mathbf{r})$, where $U(\mathbf{r})$ is an on-site random potential uniformly distributed on $[-W, W]$.

We numerically compute the zero-temperature conductance $G = \frac{e^2}{h}\mathrm{Tr}[\Gamma_L G^r \Gamma_R G^a]$ using the Landauer−Büttiker formula,[57] where $G^r(E_F) = [G^a(E_F)]^\dagger = [E_F - H - \sum_L - \sum_R]^{-1}$ is the retarded Green's function, $\Gamma_{L/R} = i[\sum_{L/R}^r - \sum_{L/R}^a]$ is the line width function, and $\sum_{L/R}$ is the self-energy of the left/right lead. The conductance fluctuation δG is calculated as the standard deviation of conductance G for an ensemble of disorder, $\delta G = \langle (G - \langle G \rangle)^2 \rangle^{1/2}$, averaged over at least 200 ensembles. In the calculation, we use $M_0 = -0.4$, $M_z = M_x = M_y = -0.5$, and $A = D = 1$ and use a quasi-1-dimensional system with sizes $L_x = 10$, $L_y = 30$, and $L_z = 100$. The magnitude of the UCF is determined as the average value over the plateau where conductance fluctuations saturate as the disorder strength is varied. We further confirm the convergence of the UCF magnitude by testing its sensitivity to the system size L_α, $\alpha = x, y, z$. This method ensures that the UCF obtained are universal values in the diffusive regime and also helps get rid of the finite size effect in numerical calculations.

As shown in Figure 3c, when the magnetic flux per unit cell, normalized with the magnetic flux quanta (ϕ/ϕ_0), goes beyond a critical value, the UCF magnitude decreases by $\sqrt{2}$, both close to and away from the charge neutrality point. Thus, our observed reduction in the magnitude of UCF by a factor of $\sqrt{2}$ is consistent with that predicted theoretically for Dirac materials. It is important to emphasize that although the parameters used in the model may not be realistic for the experiments, they are sufficient to capture the correct transitions of the intrinsic magnitude of the UCF between symmetry classes. This is because the transition depends on the symmetry class of the Hamiltonian and not on the details of the Hamiltonian parameters, such as the strength of spin−orbital coupling, the effective band mass, etc. However, our theory is unable to capture the critical magnetic field beyond which the magnitude of the UCF changes its intrinsic value, as it depends on various system parameters other than the symmetry indices such as the system length used in the calculation. We also note that previous experiments on mesoscopic Cd_3As_2 channels showed a $2\sqrt{2}$ reduction.[23] This may be caused by factors such as magnetic-field-induced gap or decoherence.[26] Quantum confinement, which can open up a small gap at the Dirac point in films of the thickness we used (∼20 nm), may also play a role here, since the thickness of our films is much smaller than the nanowires investigated in the previous experiment (∼100 nm). The role of disorder is also not clear, which leads to the removal of valley degeneracy and can affect the magnitude of the UCF.

To evaluate the impact of an externally applied electric field on UCF, we extracted the rms magnitude as a function of V_g, which is plotted in Figure 4a. We observe a strong suppression

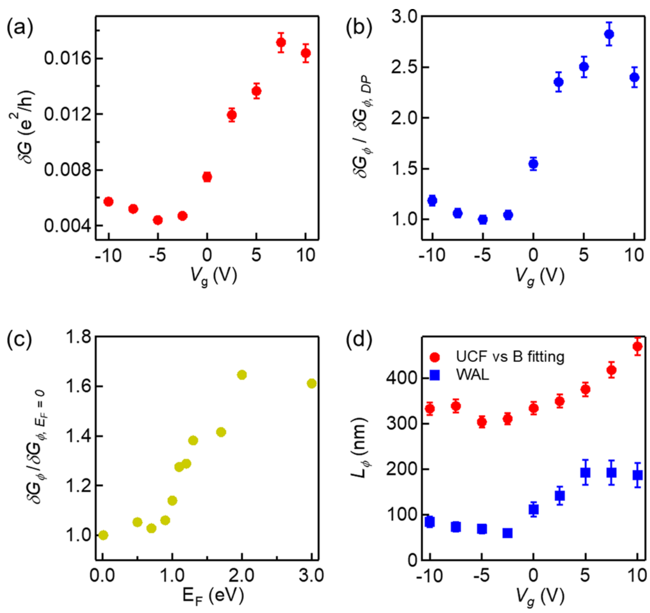

Figure 4. Gate-voltage dependence of UCF. (a) rms magnitude of the fluctuations as a function of gate voltage (V_g). (b) Magnitude of the UCF within a phase-coherent box, showing an increase by a factor of 2.5 as V_g is tuned away from the charge neutrality point. (c) Numerically calculated normalized magnitude of UCF within a phase-coherent box as a function of the Fermi energy. (d) Comparison of the phase breaking length (L_ϕ) obtained from different methods.

of UCF near the charge neutrality point. The suppression of UCF at the charge neutrality point was observed in prior studies of topological insulators and Dirac semimetals. This was attributed to an increase in l_ϕ at high carrier densities due to the screening of impurity scattering potential,[23,38,58] although the trend within a phase-coherent box was not investigated. In the context of single-layer graphene, although δG shows a decrease or increase at higher Fermi energy (E_f), the magnitude within a phase-coherent box (δG_ϕ) decreases by a factor of 4 away from the Dirac point, due to the removal of valley degeneracy.[59] To probe this further, we evaluated the UCF magnitude within a phase-coherent box by using $\delta G_\phi^2 = LW\frac{\delta G^2}{L_\phi^2}$.[36] We observe an increase in the magnitude

https://doi.org/10.1021/acs.nanolett.3c01174
Nano Lett. 2023, 23, 5634−5640

(normalized with the value at the Dirac point, $\delta G_{\phi,\mathrm{DP}}$) as V_g is tuned away from the Dirac point (Figure 4b), by a factor of 2.5 in this device (see sections SIII and SIV in the Supporting Information). This trend of increasing magnitude of UCF with increasing E_f is also captured in our numerical calculation, as shown in Figure 4c, where we plot the normalized UCF magnitude as a function of E_f. We attribute this increase of UCF to Fermi surface anisotropy. The strong anisotropy of the Fermi surface around the Dirac point is an important feature of Cd_3As_2 and can be described correctly by the effective low-energy Hamiltonian $H_0(\mathbf{k})$ in eq 3.[41,60] The effects of Fermi surface anisotropy can be intuitively understood as follows: we neglect the $D\mathbf{k}_\pm$ terms in $H_0(\mathbf{k})$ and locate the Dirac point at $(0, 0, \sqrt{M_0/M_z})$. The states around the Dirac point have much longer wavelength $\lambda_\alpha = \frac{2\pi}{k_\alpha}$ along the $\alpha = x, y$ direction than along the z direction. Thus, the electrons effectively travel in a 1-dimensional system rather than in a 3-dimensional system. UCFs are suppressed through the reduction of the prefactor from $c_{d=3}$ to $c_{d=1}$ in the formula $\delta G = c_d\sqrt{\frac{ks^2}{\beta}}$. Away from the Dirac point, electrons recover the 3-dimensional transport and the UCF increase due to the increase of the prefactor c_d. This is validated in the numerical calculation, where we have used a cube of size $L_x = L_y = L_z = 12$ to describe a phase-coherent region inside the material. We emphasize here that the effect of Fermi surface anisotropy depends on realistic parameters and can only be described qualitatively through the model assumed in this manuscript; a quantitative understanding of the influence of the Fermi-surface anisotropy on the UCF still needs further study.

Finally, we extracted the V_g dependence of L_ϕ from two independent methods: (a) we determine via the magnetoresistance by using fits to the HLN equation (eq 1) and (b) we directly determine L_ϕ from the UCF by analyzing the autocorrelation function[23,61]

$$F(\Delta B) = \frac{\langle \delta G(B)\delta G(B + \Delta B)\rangle_B}{\langle \delta G^2\rangle}$$

We use this to obtain the correlation field B_0 using the equation $F(B_0) = 0.5F(0)$ and then determine $L_\phi = 2.4\left(\frac{h}{eB_0}\right)^{1/2}$.

We find that the values of L_ϕ determined from magnetoresistance and UCF differ in magnitude by a factor of 3 over the V_g range that has been investigated (Figure 4d). We also find L_ϕ increases away from the Dirac point in both cases. Enhanced screening of electromagnetic fluctuations at higher number densities leads to a larger L_ϕ away from the Dirac point, while inhomogeneity from electron−hole puddles leads to lower L_ϕ around the Dirac point.[38,62,63] The factor of 3 difference in L_ϕ obtained from the two methods has two possible explanations. First, the phase breaking time τ_ϕ relevant for weak localization (WL) is related to the Nyquist dephasing rate, while the scattering time scale for UCF depends on the outscattering time, which is related to the inverse of the inelastic collision frequency.[64,65] The influence of these two mechanisms on dephasing can differ, and this difference has been investigated in a variety of samples.[38,49,50,55,66−70] Further investigation is required to identify whether both WL and UCF are governed by the same scattering rates in Dirac materials.

In conclusion, we have investigated UCF in mesoscopic transport channels of Dirac semimetal Cd_3As_2. We find that the magnitude of UCF is reduced by a factor of $\sqrt{2}$ as the magnetic field is increased due to the removal of time-reversal symmetry. Our observations are consistent with a topological phase transition from the symplectic to unitary symmetry class. We also find that the magnitude of UCF increases as the Fermi energy in the system is increased, which we attribute to Fermi surface anisotropy rather than broken inversion symmetry. Our experiments establish UCF to be the intrinsic source of fluctuations in these systems and emphasize their importance in probing phase-coherent transport. The good concurrence between theoretical predictions and experimental observations indicates that measurements of UCF provide a promising route for rigorously probing the influence of broken symmetry on the band structure of topological quantum materials.

■ ASSOCIATED CONTENT

Supporting Information

The Supporting Information is available free of charge at https://pubs.acs.org/doi/10.1021/acs.nanolett.3c01174.

Key features of UCF, magnetoresistance data of Dev I and II, gate-voltage dependence of Dev I, magnetic field and gate-voltage dependence of UCF in Dev II (PDF)

■ AUTHOR INFORMATION

Corresponding Authors

Saurav Islam − *Department of Physics, Pennsylvania State University, University Park, Pennsylvania 16802, United States*; Email: ski5160@psu.edu

Nitin Samarth − *Department of Physics, Pennsylvania State University, University Park, Pennsylvania 16802, United States*; orcid.org/0000-0003-2599-346X; Email: nxs16@psu.edu

Authors

Run Xiao − *Department of Physics, Pennsylvania State University, University Park, Pennsylvania 16802, United States*

Wilson Yanez − *Department of Physics, Pennsylvania State University, University Park, Pennsylvania 16802, United States*

Yongxi Ou − *Department of Physics, Pennsylvania State University, University Park, Pennsylvania 16802, United States*

Haiwen Liu − *Center for Advanced Quantum Studies, Department of Physics, Beijing Normal University, Beijing 100875, People's Republic of China*

Xincheng Xie − *International Center for Quantum Materials, School of Physics, Peking University, Beijing 100871, People's Republic of China; Hefei National Laboratory, Hefei 230088, People's Republic of China*

Juan Chamorro − *Department of Chemistry, Johns Hopkins University, Baltimore, Maryland 21218, United States*

Tyrel M. McQueen − *Department of Chemistry, Johns Hopkins University, Baltimore, Maryland 21218, United States*; orcid.org/0000-0002-8493-4630

Complete contact information is available at: https://pubs.acs.org/10.1021/acs.nanolett.3c01174

Notes

The authors declare no competing financial interest.

■ ACKNOWLEDGMENTS

The authors thank Yayun Hu for invaluable technical contributions to the theoretical calculations in this paper. This project was supported by the Institute for Quantum Matter under DOE EFRC Grant No. DESC0019331. The Penn State Two-Dimensional Crystal Consortium Materials Innovation Platform (2DCC-MIP) under NSF Grant No. DMR-2039351 provided support for ARPES measurements. W.Y. acknowledges support from the Penn State Materials Research Science and Engineering Center for Nanoscale Science under NSF Grant No. DMR-2011839. We also thank the Penn State Eberly College of Science for support (S.I., N.S.).

■ REFERENCES

(1) Hasan, M. Z.; Kane, C. L. Colloquium: topological insulators. *Rev. Mod. Phys.* **2010**, *82*, 3045.
(2) Samarth, N. Quantum materials discovery from a synthesis perspective. *Nat. Mater.* **2017**, *16*, 1068−1076.
(3) Yan, B.; Felser, C. Topological materials: Weyl semimetals. *Annu. Rev. Condens. Matter Phys.* **2017**, *8*, 337−354.
(4) Wen, X.-G. Colloquium: Zoo of quantum-topological phases of matter. *Rev. Mod. Phys.* **2017**, *89*, 041004.
(5) Armitage, N. P.; Mele, E. J.; Vishwanath, A. Weyl and Dirac semimetals in three-dimensional solids. *Rev. Mod. Phys.* **2018**, *90*, 015001.
(6) Xiong, J.; Kushwaha, S. K.; Liang, T.; Krizan, J. W.; Hirschberger, M.; Wang, W.; Cava, R. J.; Ong, N. P. Evidence for the chiral anomaly in the Dirac semimetal Na_3Bi. *Science* **2015**, *350*, 413−416.
(7) Shekhar, C.; et al. Extremely large magnetoresistance and ultrahigh mobility in the topological Weyl semimetal candidate NbP. *Nat. Phys.* **2015**, *11*, 645−649.
(8) Huang, X.; Zhao, L.; Long, Y.; Wang, P.; Chen, D.; Yang, Z.; Liang, H.; Xue, M.; Weng, H.; Fang, Z.; Dai, X.; Chen, G. Observation of the chiral-anomaly-induced negative magnetoresistance in 3D Weyl semimetal TaAs. *Phys. Rev. X* **2015**, *5*, 031023.
(9) Liang, T.; Gibson, Q.; Ali, M. N.; Liu, M.; Cava, R. J.; Ong, N. P. Ultrahigh mobility and giant magnetoresistance in the Dirac semimetal Cd_3As_2. *Nat. Mater.* **2015**, *14*, 280−284.
(10) Zhang, C.-L.; Xu, S.-Y.; Belopolski, I.; Yuan, Z.; Lin, Z.; Tong, B.; Bian, G.; Alidoust, N.; Lee, C.-C.; Huang, S.-M.; et al. Signatures of the Adler−Bell−Jackiw chiral anomaly in a Weyl fermion semimetal. *Nat. Commun.* **2016**, *7*, 1−9.
(11) Collins, J. L.; Tadich, A.; Wu, W.; Gomes, L. C.; Rodrigues, J. N.; Liu, C.; Hellerstedt, J.; Ryu, H.; Tang, S.; Mo, S.-K.; Adam, S.; Yang, S.; Fuhrer, M. S.; Edmonds, M. T. Electric-field-tuned topological phase transition in ultrathin Na_3Bi. *Nature* **2018**, *564*, 390−394.
(12) Ong, N. P.; Liang, S. Experimental signatures of the chiral anomaly in Dirac-Weyl semimetals. *Nat. Rev. Phys.* **2021**, *3*, 394−404.
(13) Di Bernardo, I.; Hellerstedt, J.; Liu, C.; Akhgar, G.; Wu, W.; Yang, S. A.; Culcer, D.; Mo, S.-K.; Adam, S.; Edmonds, M. T.; Fuhrer, M. S. Progress in Epitaxial Thin-Film Na_3Bi as a Topological Electronic Material. *Adv. Mater.* **2021**, *33*, 2005897.
(14) Wang, Z.; Weng, H.; Wu, Q.; Dai, X.; Fang, Z. Three-dimensional Dirac semimetal and quantum transport in Cd_3As_2. *Phys. Rev. B* **2013**, *88*, 125427.
(15) Uchida, M.; Nakazawa, Y.; Nishihaya, S.; Akiba, K.; Kriener, M.; Kozuka, Y.; Miyake, A.; Taguchi, Y.; Tokunaga, M.; Nagaosa, N.; Tokura, Y.; Kawasaki, M. Quantum Hall states observed in thin films of Dirac semimetal Cd_3As_2. *Nat. Commun.* **2017**, *8*, 2274.
(16) Schumann, T.; Galletti, L.; Kealhofer, D. A.; Kim, H.; Goyal, M.; Stemmer, S. Observation of the quantum Hall effect in confined films of the three-dimensional Dirac semimetal Cd_3As_2. *Phys. Rev. Lett.* **2018**, *120*, 016801.
(17) Kealhofer, D. A.; Galletti, L.; Schumann, T.; Suslov, A.; Stemmer, S. Topological insulator state and collapse of the quantum Hall effect in a three-dimensional Dirac semimetal heterojunction. *Phys. Rev. X* **2020**, *10*, 011050.
(18) Kealhofer, D. A.; Kealhofer, R.; Ohara, D.; Pardue, T. N.; Stemmer, S. Controlling and visualizing Dirac physics in topological semimetal heterostructures. *Sci. Adv.* **2022**, *8*, No. eabn4479.
(19) Yanez, W.; et al. Spin and Charge Interconversion in Dirac-Semimetal Thin Films. *Phys. Rev. Applied* **2021**, *16*, 054031.
(20) Xiao, R.; Zhang, J.; Chamorro, J.; Kim, J.; McQueen, T. M.; Vanderbilt, D.; Kayyalha, M.; Li, Y.; Samarth, N. Integer quantum Hall effect and enhanced *g* factor in quantum-confined Cd_3As_2 films. *Phys. Rev. B* **2022**, *106*, L201101.
(21) Li, C.-Z.; Wang, L.-X.; Liu, H.; Wang, J.; Liao, Z.-M.; Yu, D.-P. Giant negative magnetoresistance induced by the chiral anomaly in individual Cd_3As_2 nanowires. *Nat. Commun.* **2015**, *6*, 1−7.
(22) Moll, P. J.; Nair, N. L.; Helm, T.; Potter, A. C.; Kimchi, I.; Vishwanath, A.; Analytis, J. G. Transport evidence for Fermi-arc-mediated chirality transfer in the Dirac semimetal Cd_3As_2. *Nature* **2016**, *535*, 266−270.
(23) Wang, L.-X.; Wang, S.; Li, J.-G.; Li, C.-Z.; Yu, D.; Liao, Z.-M. Universal conductance fluctuations in Dirac semimetal Cd_3As_2 nanowires. *Phys. Rev. B* **2016**, *94*, No. 161402.
(24) Rashidi, A.; Kealhofer, R.; Lygo, A. C.; Stemmer, S. Universal conductance fluctuations in nanoscale topological insulator devices. *Appl. Phys. Lett.* **2023**, *122*, 053101.
(25) Zheng, G.; Zhu, X.; Liu, Y.; Lu, J.; Ning, W.; Zhang, H.; Gao, W.; Han, Y.; Yang, J.; Du, H.; Yang, K.; Zhang, Y.; Tian, M. Field-induced topological phase transition from a three-dimensional Weyl semimetal to a two-dimensional massive Dirac metal in $ZrTe_5$. *Phys. Rev. B* **2017**, *96*, No. 121401.
(26) Hu, Y.; Liu, H.; Jiang, H.; Xie, X. C. Numerical study of universal conductance fluctuations in three-dimensional topological semimetals. *Phys. Rev. B* **2017**, *96*, 134201.
(27) Lee, P. A.; Stone, A. D. Universal conductance fluctuations in metals. *Phys. Rev. Lett.* **1985**, *55*, 1622.
(28) Feng, S.; Lee, P. A.; Stone, A. D. Sensitivity of the Conductance of a Disordered Metal to the Motion of a Single Atom: Implications for 1/f Noise. *Phys. Rev. Lett.* **1986**, *56*, 1960.
(29) Altshuler, B. L.; Shklovskii, B. I. Repulsion of energy levels and the conductance of small metallic samples. *Zh. Eksp. Teor. Fiz.* **1986**, *91*, 220−234.
(30) Altshuler, B. L. Fluctuations in the extrinsic conductivity of disordered conductors. *Pis'ma Zh. Eksp. Teor. Fiz.* **1985**, *41*, 530−533.
(31) Altshuler, B. L.; Spivak, B. Z. Variation of random potential and the conductivity of samples of small dimensions. *Pis'ma Zh. Eksp. Teor. Fiz.* **1985**, *42*, 363−365.
(32) Dyson, F. J. Statistical theory of the energy levels of complex systems. *J. Math. Phys.* **1962**, *3*, 140−156.
(33) Beenakker, C. W. J. Random-matrix theory of quantum transport. *Rev. Mod. Phys.* **1997**, *69*, 731.
(34) Ghosh, A.; Raychaudhuri, A. K. Universal conductance fluctuations in three dimensional metallic single crystals of Si. *Phys. Rev. Lett.* **2000**, *84*, 4681.
(35) Mehta, M. L. *Random matrices*; Elsevier: 2004; Vol. *142*; pp 1−688.
(36) Pal, A. N.; Kochat, V.; Ghosh, A. Direct observation of valley hybridization and universal symmetry of graphene with mesoscopic conductance fluctuations. *Phys. Rev. Lett.* **2012**, *109*, 196601.
(37) Shamim, S.; Mahapatra, S.; Scappucci, G.; Klesse, W.; Simmons, M.; Ghosh, A. Spontaneous breaking of time-reversal symmetry in strongly interacting two-dimensional electron layers in silicon and germanium. *Phys. Rev. Lett.* **2014**, *112*, 236602.
(38) Islam, S.; Bhattacharyya, S.; Nhalil, H.; Elizabeth, S.; Ghosh, A. Universal conductance fluctuations and direct observation of crossover of symmetry classes in topological insulators. *Phys. Rev. B* **2018**, *97*, No. 241412.
(39) Hsieh, K.; Kochat, V.; Biswas, T.; Tiwary, C. S.; Mishra, A.; Ramalingam, G.; Jayaraman, A.; Chattopadhyay, K.; Raghavan, S.;

Jain, M.; Ghosh, A. Spontaneous time reversal symmetry breaking at individual grain boundaries in graphene. *Phys. Rev. Lett.* **2021**, *126*, 206803.
(40) Islam, S.; Shamim, S.; Ghosh, A. Benchmarking Noise and Dephasing in Emerging Electrical Materials for Quantum Technologies. *Adv. Mater.* **2022**, 2109671.
(41) Liu, Z. K.; et al. A stable three-dimensional topological Dirac semimetal Cd_3As_2. *Nat. Mater.* **2014**, *13*, 677−681.
(42) Borisenko, S.; Gibson, Q.; Evtushinsky, D.; Zabolotnyy, V.; Büchner, B.; Cava, R. J. Experimental realization of a three-dimensional Dirac semimetal. *Phys. Rev. Lett.* **2014**, *113*, 027603.
(43) Yi, H.; et al. Evidence of topological surface state in three-dimensional Dirac semimetal Cd_3As_2. *Sci. Rep.* **2014**, *4*, 1−6.
(44) Cheng, P.; Zhang, C.; Liu, Y.; Yuan, X.; Song, F.; Sun, Q.; Zhou, P.; Zhang, D. W.; Xiu, F. Thickness-dependent quantum oscillations in Cd_3As_2 thin films. *New J. Phys.* **2016**, *18*, 083003.
(45) Xiao, R.; Held, J. T.; Rable, J.; Ghosh, S.; Wang, K.; Mkhoyan, K. A.; Samarth, N. Challenges to magnetic doping of thin films of the Dirac semimetal Cd 3 As 2. *Phys. Rev. Mater.* **2022**, *6*, 024203.
(46) Xiao, R.; Zhang, J.; Chamorro, J.; Kim, J.; McQueen, T. M.; Vanderbilt, D.; Kayyalha, M.; Li, Y.; Samarth, N. Integer quantum Hall effect and enhanced g factor in quantum-confined Cd 3 As 2 films. *Phys. Rev. B* **2022**, *106*, L201101.
(47) Bergmann, G. Weak localization in thin films: a time-of-flight experiment with conduction electrons. *Phys. Rep.* **1984**, *107*, 1−58.
(48) Hikami, S.; Larkin, A. I.; Nagaoka, Y. Spin-orbit interaction and magnetoresistance in the two dimensional random system. *Prog. Theor. Phys.* **1980**, *63*, 707−710.
(49) Chandrasekhar, V.; Santhanam, P.; Prober, D. E. Weak localization and conductance fluctuations in complex mesoscopic geometries. *Phys. Rev. B* **1991**, *44*, 11203.
(50) McConville, P.; Birge, N. O. Weak localization, universal conductance fluctuations, and 1/f noise in Ag. *Phys. Rev. B* **1993**, *47*, 16667.
(51) Wang, J.; DaSilva, A. M.; Chang, C.-Z.; He, K.; Jain, J. K.; Samarth, N.; Ma, X.-C.; Xue, Q.-K.; Chan, M. H. W. Evidence for electron-electron interaction in topological insulator thin films. *Phys. Rev. B* **2011**, *83*, 245438.
(52) Islam, S.; Bhattacharyya, S.; Nhalil, H.; Banerjee, M.; Richardella, A.; Kandala, A.; Sen, D.; Samarth, N.; Elizabeth, S.; Ghosh, A. Low-temperature saturation of phase coherence length in topological insulators. *Phys. Rev. B* **2019**, *99*, 245407.
(53) Birge, N. O.; Golding, B.; Haemmerle, W. Electron Quantum Interference and 1 f Noise in Bismuth. *Phys. Rev. Lett.* **1989**, *62*, 195.
(54) Birge, N. O.; Golding, B.; Haemmerle, W. H. Conductance fluctuations and 1/f noise in Bi. *Phys. Rev. B* **1990**, *42*, 2735.
(55) Hoadley, D.; McConville, P.; Birge, N. O. Experimental comparison of the phase-breaking lengths in weak localization and universal conductance fluctuations. *Phys. Rev. B* **1999**, *60*, 5617.
(56) Yang, P.-Y.; Wang, L. Y.; Hsu, Y.-W.; Lin, J.-J. Universal conductance fluctuations in indium tin oxide nanowires. *Phys. Rev. B* **2012**, *85*, 085423.
(57) Datta, S. *Electronic Transport in Mesoscopic Systems*; Cambridge University Press: 1995; Cambridge Studies in Semiconductor Physics and Microelectronic Engineering/
(58) Rossi, E.; Bardarson, J. H.; Fuhrer, M. S.; Das Sarma, S. Universal conductance fluctuations in Dirac materials in the presence of long-range disorder. *Phys. Rev. Lett.* **2012**, *109*, 096801.
(59) Pal, A. N.; Kochat, V.; Ghosh, A. Direct Observation of Valley Hybridization and Universal Symmetry of Graphene with Mesoscopic Conductance Fluctuations. *Phys. Rev. Lett.* **2012**, *109*, 196601.
(60) Zhao, Y.; Liu, H.; Zhang, C.; Wang, H.; Wang, J.; Lin, Z.; Xing, Y.; Lu, H.; Liu, J.; Wang, Y.; Brombosz, S. M.; Xiao, Z.; Jia, S.; Xie, X. C.; Wang, J. Anisotropic Fermi surface and quantum limit transport in high mobility three-dimensional Dirac semimetal Cd_3As_2. *Phys. Rev. X* **2015**, *5*, 031037.
(61) Vila, L.; Giraud, R.; Thevenard, L.; Lemaître, A.; Pierre, F.; Dufouleur, J.; Mailly, D.; Barbara, B.; Faini, G. Universal conductance fluctuations in epitaxial GaMnAs ferromagnets: Dephasing by structural and spin disorder. *Phys. Rev. Lett.* **2007**, *98*, 027204.
(62) Chiu, S.-P.; Lin, J.-J. Weak antilocalization in topological insulator Bi_2Te_3 microflakes. *Phys. Rev. B* **2013**, *87*, 035122.
(63) Tian, J.; Chang, C.; Cao, H.; He, K.; Ma, X.; Xue, Q.; Chen, Y. P. Quantum and classical magnetoresistance in ambipolar topological insulator transistors with gate-tunable bulk and surface conduction. *Sci. Rep.* **2014**, *4*, 4859.
(64) Altshuler, B. L.; Aronov, A. G.; Khmelnitsky, D. E. Effects of electron-electron collisions with small energy transfers on quantum localisation. *J. Phys. C: Solid State Phys.* **1982**, *15*, 7367.
(65) Blanter, Y. M. Electron-electron scattering rate in disordered mesoscopic systems. *Phys. Rev. B* **1996**, *54*, 12807.
(66) Hoadley, D.; McConville, P.; Birge, N. O. Experimental comparison of the phase-breaking lengths in weak localization and universal conductance fluctuations. *Phys. Rev. B* **1999**, *60*, 5617−5625.
(67) Aleiner, I. L.; Blanter, Y. M. Inelastic scattering time for conductance fluctuations. *Phys. Rev. B* **2002**, *65*, 115317.
(68) Trionfi, A.; Lee, S.; Natelson, D. Electronic coherence in metals: Comparing weak localization and time-dependent conductance fluctuations. *Phys. Rev. B* **2004**, *70*, No. 041304.
(69) Trionfi, A.; Lee, S.; Natelson, D. Time-dependent universal conductance fluctuations and coherence in AuPd and Ag. *Phys. Rev. B* **2005**, *72*, 035407.
(70) Shamim, S.; Mahapatra, S.; Scappucci, G.; Klesse, W. M.; Simmons, M. Y.; Ghosh, A. Dephasing rates for weak localization and universal conductance fluctuations in two dimensional Si: P and Ge: P δ-layers. *Sci. Rep.* **2017**, *7*, 1−9.

Recommended by ACS

Universal Conductance Fluctuations in a $MnBi_2Te_4$ Thin Film
Molly P. Andersen, David Goldhaber-Gordon, *et al.*
NOVEMBER 29, 2023
NANO LETTERS
READ

Observation of Anomalous Planar Hall Effect Induced by One-Dimensional Weak Antilocalization
Jingyuan Zhong, Weichang Hao, *et al.*
JANUARY 26, 2024
ACS NANO
READ

Chern-Insulator Phase in Antiferromagnets
Yuntian Liu, Qihang Liu, *et al.*
SEPTEMBER 13, 2023
NANO LETTERS
READ

Controlling the Interlayer Dzyaloshinskii–Moriya Interaction by Electrical Currents
Fabian Kammerbauer, Mathias Kläui, *et al.*
JULY 19, 2023
NANO LETTERS
READ

Get More Suggestions >